
P-Guide: Parameter-Efficient Prior Steering for Single-Pass CFG Inference

Xin Peng¹ Ang Gao^{1*}

¹School of Physical Science and Technology,
Beijing University of Posts and Telecommunications, Beijing, China
anggao@bupt.edu.cn

Abstract

Classifier-Free Guidance (CFG) is essential for high-fidelity conditional generation in flow matching, yet it imposes significant computational overhead by requiring dual forward passes at each sampling step. In this work, we address this bottleneck by introducing **P-Guide**, a framework that achieves high-quality guidance through a single inference pass by modulating only the initial latent state. We further show that, under a first-order approximation, P-Guide is equivalent to CFG in the sense that it steers generation from the prior space, without requiring explicit velocity field extrapolation during sampling. We consider both homoscedastic and **heteroscedastic** priors, and find that jointly modeling the mean and variance enables adaptive loss attenuation and improved robustness to data uncertainty. Extensive experiments demonstrate that P-Guide reduces inference latency by approximately 50% while maintaining fidelity and prompt alignment competitive with standard dual-pass CFG baselines.

1 Introduction

Continuous-time generative modeling frameworks, such as Flow Matching (FM) [23, 1] and Rectified Flow [25], have established a powerful paradigm for transforming simple prior distributions into complex data manifolds via deterministic Ordinary Differential Equations (ODEs) [42, 41]. This line of methods is closely connected to score-based diffusion models [18, 40, 27], and has recently progressed toward scalable generative architectures, combining flow-based modeling paradigms with transformer-based architectures [29, 12].

To achieve precise semantic control in large-scale text-to-image synthesis, Classifier-Free Guidance (CFG) [17] has become an indispensable technique in modern generative systems, including Stable Diffusion [33], SDXL [30], Imagen [35], DALL-E 2 [32], DALL-E [31], GLIDE [28], and recent industrial-scale models such as Stable Diffusion 3 / 3.5 [12, 3], FLUX [4], and large multimodal systems like Qwen-Image [7] and Wanxiang [45]. By linearly extrapolating between conditional and unconditional velocity fields, CFG significantly sharpens prompt alignment and enhances structural fidelity across diffusion and flow-based architectures [11, 12].

Despite its success, the standard implementation of CFG faces a major computational bottleneck: the dual-pass requirement. At each sampling step, the model must be evaluated twice—once for the conditional branch and once for the unconditional one. This doubles the inference latency and remains the primary obstacle for deploying high-fidelity generative flows in real-time or resource-constrained environments, especially in large-scale systems such as SDXL [30], SD3 [12], and FLUX [4]. While existing methods attempt to mitigate this via distillation or step-truncation [37, 47, 43, 26], they often require intensive retraining or compromise the geometric consistency of the generation path.

*Corresponding author

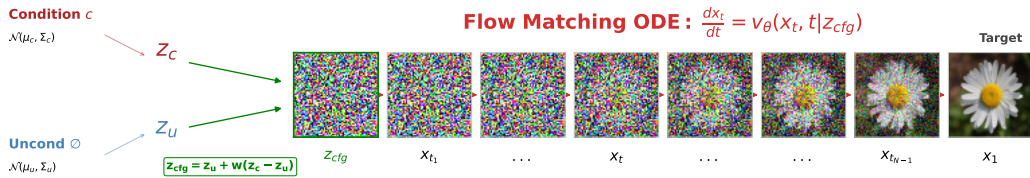


Figure 1: **Conceptual overview of the P-Guide framework.** Standard CFG requires evaluating the velocity field twice (v_{cond}, v_{uncond}) at each integration step. P-Guide relocates this guidance to the origin by modulating the initial noise state using a data-dependent prior. Based on our trajectory-level approximation, this initial shift anchors the global ODE path, enabling high-fidelity conditional generation with only a **single inference pass**.

In this work, we propose to mitigate this bottleneck by shifting the guidance mechanism from the sampling process to the trajectory origin (see Figure 1). We introduce **P-Guide** (Prior-Guide), a parameter-efficient framework that achieves conditional control by modulating the initial state in the prior space. Our approach is motivated by a **trajectory-level approximation perspective**, where we show that a structured shift in the prior space is consistent with velocity field extrapolation along the ODE trajectory under a first-order approximation. By steering the generation from its starting point, P-Guide enables high-quality guided sampling with only a **single inference pass** per step, leading to a substantial reduction in the computational cost of CFG.

Furthermore, we explore both homoscedastic and heteroscedastic formulations of the prior, where the latter jointly models the conditional mean and variance in the latent space. This allows the model to capture data-dependent uncertainty and implement an adaptive loss attenuation mechanism, improving robustness against noisy conditions. Through extensive experiments on benchmark datasets including ImageNet-1k, we demonstrate that P-Guide delivers a $2\times$ speedup in CFG inference while maintaining fidelity and prompt alignment competitive with standard dual-pass baselines, requiring only a small number of additional parameters.

Our Contributions. We shift the guidance mechanism from the sampling process to the trajectory’s origin. Our technical contributions include:

- **Trajectory-Level approximation :** A first-order analysis showing that a structured shift in the prior space is consistent with velocity field extrapolation along the ODE evolution.
- **P-Guide Framework:** A parameter-efficient approach enabling single-pass CFG inference by modulating the initial state, reducing the computational cost of guidance by 50%.
- **Heteroscedastic Modeling:** We study both homoscedastic and heteroscedastic priors, and show that joint mean-variance modeling captures data-dependent uncertainty and enables adaptive loss attenuation.

2 Related Work

Diffusion and Flow-Based Generative Models. Generative modeling has transitioned from stochastic diffusion models [18, 40, 27, 42] to continuous-time frameworks such as Flow Matching (FM) and Rectified Flow [23, 25]. While diffusion models rely on iterative score estimation to reverse a noising process, FM instead regresses a time-dependent velocity field to transport a simple prior toward the data manifold [23]. Rectified Flow further improves efficiency by learning near-straight trajectories, thereby reducing discretization errors in Ordinary Differential Equation (ODE) solvers [25]. These approaches have recently been extended to large-scale transformer-based generative models [29, 12].

Informed and Data-Dependent Priors. Beyond standard uninformed priors, recent works demonstrate that context-aware distributions can enhance conditioning efficiency and reduce transport complexity [22, 24, 5, 39]. Specifically, PriorGrad [22] and Warm-Start Diffusion [39] adapt priors to conditional statistics to simplify the generative task, while CAR-Flow [5] and CrossFlow [24]

relocate distributions via learned shifts or cross-modal mappings to align source and target manifolds. Despite improving training convergence or modeling flexibility, these techniques do not address the inherent dual-pass computational bottleneck imposed by classifier-free guidance during inference.

Conditional Generative Modeling and Classifier-Free Guidance. Classifier-Free Guidance (CFG) [17] has become the de facto standard for controllable generation, enhancing semantic alignment by extrapolating between conditional and unconditional predictions. It is widely adopted in modern text-to-image systems, including Stable Diffusion [33], SDXL [30], and more recent flow-based large-scale models such as Stable Diffusion 3 [12] and FLUX [4]. However, the standard implementation requires two forward passes per sampling step, doubling inference cost and limiting deployment in real-time or resource-constrained settings.

Analysis and Control of Guidance Dynamics. Recent work has investigated the geometric properties and stability of guided sampling trajectories. CFG-Zero* [13] improves early-stage guidance behavior via optimized scaling, while CFG-MP [8] and Rectified-CFG++ [36] incorporate manifold constraints or predictor–corrector schemes to maintain trajectory consistency. CFG-Ctrl [46] further formulates guidance as a control problem, providing a dynamical systems perspective. More recently, C²FG [14] analyzes guidance through score discrepancy and introduces a principled control mechanism to stabilize conditional generation. Nevertheless, these methods primarily modify the guidance dynamics within the sampling trajectory and do not eliminate the inherent dual-pass computational bottleneck of CFG.

3 Background

3.1 Flow Matching

Flow Matching (FM) provides a simulation-free framework to train continuous normalizing flows by regressing a time-dependent velocity field $v_\theta(x_t, t)$ [23]. Given a source distribution p_0 (typically standard Gaussian) and a target data distribution p_1 , FM constructs a probability path p_t that transports p_0 to p_1 , and is closely related to diffusion models and score-based generative modeling [18, 42, 40].

The sample trajectory x_t is governed by the following ODE:

$$\frac{dx_t}{dt} = v_\theta(x_t, t), \quad x_0 \sim p_0. \quad (1)$$

For a pair of samples (x_0, x_1) , a commonly used construction is the independent conditional probability path, which uses linear interpolation: $x_t = (1-t)x_0 + tx_1$ [23]. The corresponding target velocity is constant: $u_t(x_t|x_0, x_1) = x_1 - x_0$. The model is trained using the Flow Matching objective:

$$\mathcal{L}_{FM}(\theta) = \mathbb{E}_{t, x_0, x_1} [\|v_\theta(x_t, t) - (x_1 - x_0)\|^2]. \quad (2)$$

Rectified Flow is a special case of Flow Matching that encourages straight-line trajectories to reduce numerical integration error and improve sampling efficiency [25]. Recent extensions further connect FM with transformer-based diffusion models and large-scale generative systems [29, 12].

3.2 Classifier-Free Guidance (CFG)

Classifier-Free Guidance (CFG) is the dominant technique for controllable generative modeling in diffusion and flow-based systems [17]. It has become a core component in modern text-to-image systems such as Stable Diffusion [33], SDXL [30], Imagen [35], DALL·E 2 [32], GLIDE [28], and recent large-scale models including Stable Diffusion 3 [12] and FLUX [4].

During training, the condition is randomly replaced with a null token \emptyset , allowing a single model to learn both conditional velocity $v(x_t, t|y)$ and unconditional velocity $v(x_t, t|\emptyset)$. At inference time, the guided velocity field is computed as:

$$v_{cfg}(x_t, t) = v_\theta(x_t, t|\emptyset) + w(v_\theta(x_t, t|y) - v_\theta(x_t, t|\emptyset)), \quad (3)$$

where $w \geq 1$ is the guidance scale [17]. While CFG significantly improves semantic alignment and sample fidelity, it requires evaluating the neural network twice at every integration step, which doubles computational cost and limits real-time deployment in large-scale systems such as SDXL and FLUX [30, 4].

4 Method

In this section, we present the **P-Guide** (Prior-Guide) framework. Our core innovation lies in shifting the guidance mechanism from computationally expensive velocity field extrapolation to a structured modulation of the initial state in the prior space.

4.1 Prior Space Parameterization

Standard generative flows typically transport an uninformed Gaussian prior $p_0(z) = \mathcal{N}(0, \mathbf{I})$ to a target data distribution p_1 [18, 23]. However, recent studies have shown that Gaussian priors are not strictly necessary, and learned or data-dependent priors can significantly improve conditioning efficiency and reduce transport complexity [22, 24, 5, 39].

To enable early-stage steering, we parameterize the prior distribution as $p_0(z|y)$ such that the starting point of the trajectory already encodes conditional information.

Homoscedastic P-Guide (Base). We first define a baseline modeling scheme where the condition y modulates only the mean of the prior distribution while keeping a fixed unit variance:

$$z = \epsilon + \mu_\phi(y), \quad \epsilon \sim \mathcal{N}(0, \mathbf{I}). \quad (4)$$

Under standard regression optimality (see Appendix A for details), the learnable mapping $\mu_\phi(y)$ approximates the conditional expectation $\mathbb{E}[x | y]$. We define $z_c = \epsilon + \mu_\phi(y)$ and $z_u = \epsilon + \mu_\phi(\emptyset)$, so that the initial state shift $z_c - z_u = \mu_\phi(y) - \mu_\phi(\emptyset)$ serves as a directional anchor for the global trajectory.

Heteroscedastic P-Guide (Extension). We extend the above formulation to a heteroscedastic prior, where the condition additionally controls the scale of the latent initialization. Specifically, we parameterize the conditional distribution using neural networks $(\mu_\phi(y), \sigma_\phi(y))$ and define:

$$z = \mu_\phi(y) + \sigma_\phi(y) \odot \epsilon, \quad \epsilon \sim \mathcal{N}(0, \mathbf{I}). \quad (5)$$

Here, the initial state z is no longer mere white noise but a "semantic seed" encoding the target mode. We define the conditional seed as $z_c = \mu_\phi(y) + \sigma_\phi(y) \odot \epsilon$ and the unconditional seed as $z_u = \mu_\phi(\emptyset) + \sigma_\phi(\emptyset) \odot \epsilon$, where \emptyset represents the null condition.

4.2 Sequential Two-Stage Training Paradigm

We propose a decoupled training strategy inspired by probabilistic modeling and heteroscedastic regression [19], which ensures the prior steering module captures accurate data statistics before the backbone flow model learns transport dynamics [23].

Stage 1: Heteroscedastic Prior Learning. In the first stage, we train the prior module to minimize the conditional negative log-likelihood (NLL) of the target data x_1 given condition y . This formulation

Algorithm 1 P-Guide: Training

```
# Stage 1: train F_phi
x1, y = sample_data()
mu, sigma = F_phi(y)
loss_prior = (norm(x1 - mu)** 2) / (2
    * sigma** 2)
    + 0.5 * log(sigma** 2)

# Stage 2: train v_theta
x1, y = sample_data()
eps = randn_like(x1)
mu, sigma = F_phi(y)
z = mu + sigma * eps

t = sample_uniform()
x_t = (1 - t) * z + t * x1

loss = metric(v_theta(x_t,t) - (x1 - z))
```

Algorithm 2 P-Guide: Sampling

```
# classifier- free guidance in latent
eps = randn(x_shape)
mu_c, sigma_c = F_phi(y)
mu_u, sigma_u = F_phi(None)
z = mu_u + w* (mu_c - mu_u)
z = z + (sigma_u + w* (sigma_c -
    sigma_u)) * eps
x = z

for t in schedule:
    x = x + v_theta(x,t) * dt
```

follows probabilistic maximum likelihood estimation under Gaussian observation noise and enables joint learning of mean and uncertainty [19]:

$$\mathcal{L}_{prior} = \mathbb{E}_{x_1, y} \left[\frac{\|x_1 - \mu_\phi(y)\|^2}{2\sigma_\phi^2(y)} + \frac{1}{2} \log \sigma_\phi^2(y) \right]. \quad (6)$$

This objective induces an adaptive weighting effect, where the gradient with respect to the mean estimator is scaled by the inverse of the predicted variance, thereby attenuating the influence of noisy samples. As a result, regions with high aleatoric uncertainty are down-weighted during training, leading to a more stable semantic prior representation [19].

Stage 2: Flow Matching. After convergence, we freeze the parameters and train the velocity field v_θ using a modified Flow Matching objective, where starting points z are sampled from the learned conditional prior $p_0(z|y)$ defined by the frozen module. We define the conditional probability path as $x_t = (1-t)z + tx_1$, yielding the objective:

$$\mathcal{L}_{FM}(\theta) = \mathbb{E}_{t, x_1, z \sim p_0(z|y)} [\|v_\theta(x_t, t) - (x_1 - z)\|^2]. \quad (7)$$

Since z is already aligned with condition y and geographically closer to the target manifold, the velocity field v_θ learns straighter trajectories, which is consistent with the efficiency principle of neural ODE-based generative modeling [6]. This significantly simplifies the transport task and accelerates convergence.

4.3 trajectory-level approximation

Traditional CFG operates by linearly extrapolating between conditional and unconditional velocity fields v_t at every integration step [17]. We provide an approximation perspective for P-Guide by showing that this mechanism can be interpreted as a linear shift in the prior space under the assumption of flow consistency [6, 23].

Theorem 1. *Let $\Phi_t : \mathcal{Z} \rightarrow \mathcal{X}$ be a flow map induced by a velocity field $v(x_t, t | z) = \frac{d}{dt} \Phi_t(z)$, where z denotes the initial latent state and $x_t = \Phi_t(z)$ is the trajectory at time t . We denote the trajectories starting from the conditional and unconditional initial states as $v(x_t, t | z_c)$ and $v(x_t, t | z_u)$, respectively.*

Under a trajectory linear response assumption, where the flow responds approximately linearly to perturbations in the initial latent space, the velocity difference satisfies:

$$v(x_t, t | z_c) - v(x_t, t | z_u) \propto z_c - z_u. \quad (8)$$

The result follows from a linear response approximation of the flow dynamics, where changes in the initial latent state propagate approximately linearly along the trajectory. Here, the conditional velocity $v(x_t, t | z_c)$ and unconditional velocity $v(x_t, t | z_u)$ refer to the velocity fields induced by trajectories initialized from the conditional and unconditional latent states z_c and z_u , respectively. In this regime, their difference is governed by the difference between the corresponding initial states. A more detailed derivation based on flow linearization and connections to score-based guidance is provided in Appendix A. This perspective naturally leads to the interpretation that CFG velocity can be directly controlled by the initial latent shift.

4.4 Inference: Single-Pass CFG via Prior Steering

Leveraging the first-order equivalence established in Theorem 1, **P-Guide** performs guidance by applying CFG in the prior space before ODE integration begins, i.e., conditioning is injected into the initial latent distribution. As a result, the ODE is solved only once using a single velocity field evaluation, replacing the standard CFG procedure that requires two velocity evaluations per step during integration.

The P-Guide Core Formula: We define the guided initial state z_{cfg} by performing the linear combination of learned distribution parameters directly in the prior space:

$$z_{cfg} = \mu_\phi(\emptyset) + w(\mu_\phi(y) - \mu_\phi(\emptyset)) + [\sigma_\phi(\emptyset) + w(\sigma_\phi(y) - \sigma_\phi(\emptyset))] \odot \epsilon. \quad (9)$$

Once z_{cfg} is computed, generation proceeds by solving the probability flow ODE $\frac{dx_t}{dt} = v_\theta(x_t, t)$ starting from $x_0 = z_{cfg}$. This **single inference pass** completely avoids the need for dual model evaluations per step, reducing the computational cost of CFG by 50%.

4.5 Toy Experiment: Visualizing Trajectory Equivalence

To provide empirical intuition for the **P-Guide** framework, we conduct a 2D toy experiment. This visualization demonstrates how a structured shift at the starting point effectively anchors the global trajectory, replacing the need for iterative velocity corrections.

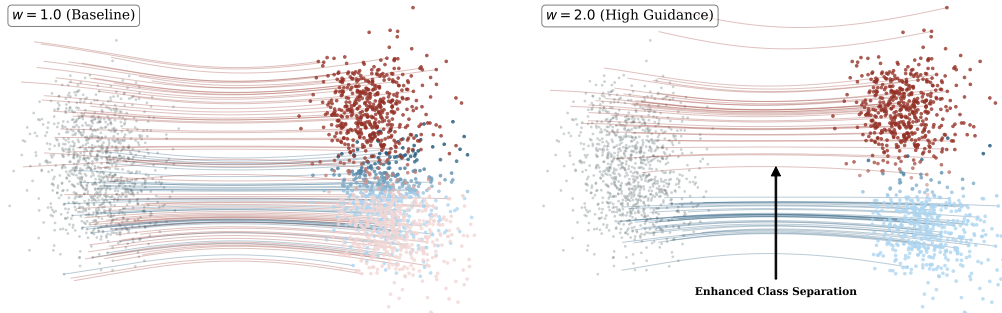


Figure 2: **Visualizing trajectory steering in a 2D toy setup.** Standard CFG requires per-step corrections in velocity space (dual-pass). P-Guide utilizes the prior shift $z_c - z_u$ as a directional anchor at $t = 0$. As shown, increasing w from 1.0 to 2.0 causes trajectories to concentrate and separate precisely toward target modes using only a **single inference pass**.

Experimental Setup. We construct a 2D dataset where the target distribution π_1 is multimodal, consisting of two distinct clusters at a radius of 5.0 units with angles of 0 and 4 radians ($\sigma = 0.5$). We train a Rectified Flow model [25] to learn the velocity field $v_\theta(x_t, t|y)$. Simultaneously, we pre-train the prior module $F_\phi(y)$ to estimate the conditional mean μ of the data clusters.

Trajectory Anchoring through Prior Steering. Standard CFG necessitates two model evaluations per step to compute an extrapolated velocity. In contrast, P-Guide injects the guidance at $t = 0$ by shifting the initial state z toward the target mode according to $z_{cfg} = z_u + w(z_c - z_u)$.

Visualizing the resulting trajectories in Figure 2 confirms that this initial shift acts as a directional anchor. Since the flow model learns to approximate straight-line transport between distributions, the semantic bias introduced at the origin naturally steers the entire deterministic ODE path. As the guidance scale w increases, the trajectories for different classes exhibit enhanced separation and concentrate more sharply on their respective target modes. This demonstrates that high-quality conditional generation is achievable through a **single inference pass**, as the trajectory is correctly anchored before sampling begins.

5 Experiments

In this section, we evaluate the empirical performance and computational efficiency of **P-Guide** across three benchmark datasets: MNIST [21], CIFAR-10 [20], and ImageNet-1k [10]. Our objective is to demonstrate that by shifting guidance to the prior space, we achieve a near-doubling of inference speed with negligible parameter overhead and no sacrifice in generation quality.

5.1 Experimental Setup

Hardware and Implementation. All experiments were conducted on a single workstation equipped with one **NVIDIA GeForce RTX 4090 GPU** (24GB VRAM). We adopt the Rectified Flow (RF) objective [25] with a linear probability path $x_t = (1 - t)z + tx_1$. For ImageNet-1k, the generative process operates in a latent space compressed by a pre-trained **AutoKL** model [12] with a storage footprint of **79.779 MB**. Following our two-stage paradigm, the prior steering module $F_\phi(y)$ is first pre-trained to convergence via Negative Log-Likelihood (NLL), consistent with probabilistic modeling in heteroscedastic regression [19]. In our main results, $F_\phi(y)$ follows the configuration described in Section 4.1, where the variance $\sigma_\phi(y)$ is learnable.

Extreme Parameter Efficiency. A key advantage of P-Guide is its extremely small parameter footprint. The proposed PG module introduces only **1.247 MB** of additional storage. This minimal overhead makes it lightweight relative to the overall generative model and enables straightforward integration into existing architectures without modifying the backbone design. We further analyze the effect of scaling the capacity of $F_\phi(y)$ in Appendix C.2.

Metrics. We report **Fréchet Inception Distance (FID)** [16], **Spatial FID (sFID)** [44], and **Inception Score (IS)** [38] to quantify sample quality. All metrics are computed using 50k generated samples following standard evaluation protocols. Efficiency is measured via hardware-agnostic **GFLOPs** per sampling step. We also report total **Model Size (MB)** to evaluate parameter efficiency.

To evaluate the effectiveness of classifier-free guidance (CFG), we further measure **generation accuracy** on conditionally generated samples. Specifically, for MNIST we use a pretrained CNN classifier achieving 99.1% accuracy [2], and for CIFAR-10 we use a pretrained ResNet-56 achieving 92.0% accuracy [15]. These classifiers are fixed and used solely to assess whether generated samples are consistent with the target labels under different guidance strengths.

5.2 Results on MNIST and CIFAR-10

For low-resolution datasets, we adopt different backbones for each setting: we use a standard **U-Net** [34, 18] for CIFAR-10, and **LightningDiT** [48] for MNIST. We compare our single-pass P-Guide against the standard dual-pass Vanilla CFG baseline. For a fair comparison, both CFM and P-Guide are trained for 400K steps under identical settings.

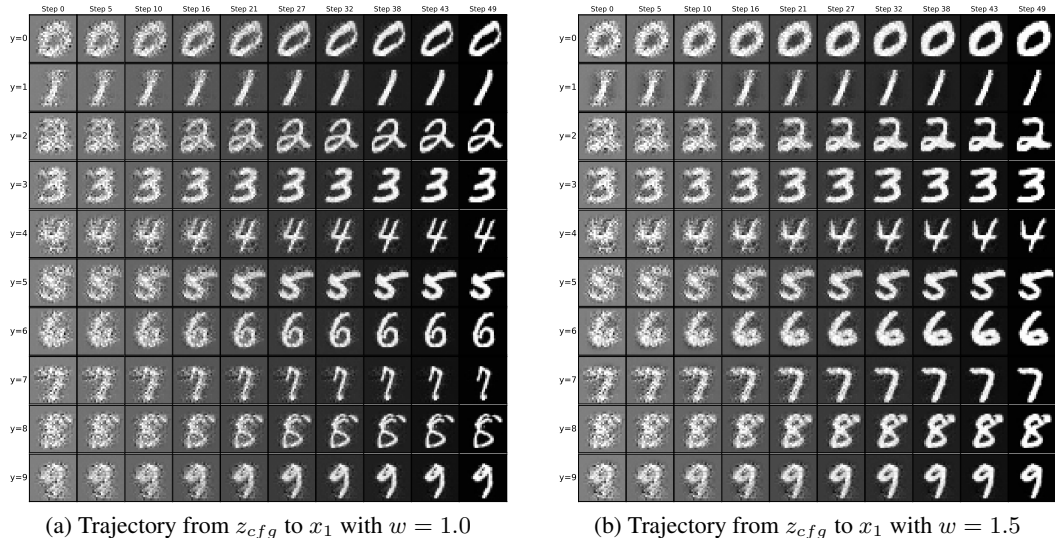


Figure 3: **Visual comparison of P-Guide generation trajectories on MNIST.** Each row shows the evolution from prior ($t = 0$) to data ($t = 1$). Increasing the guidance scale ($w = 1.0 \rightarrow 1.5$) sharpens semantic structure from early steps, confirming effective trajectory-level control from the origin.

Trajectory Generation Evolution. To intuitively understand the guidance mechanism, we visualize the step-by-step generation process of MNIST digits using the same random seed under two different guidance scales in Figure 3.

Quality and Throughput. As shown in Table 1, we sweep the guidance scale w for all methods and observe that increasing w generally improves classification accuracy, indicating stronger conditional alignment. Standard CFM achieves this by combining conditional and unconditional velocity fields at each step, but incurs a $2\times$ computational cost when $w > 1.0$ (e.g., GFLOPs increase from 417.6 to 835.2 on MNIST), whereas **P-Guide** performs guidance in prior space and maintains nearly constant computational cost across all w with negligible overhead. Around $w \approx 1.0$, the heteroscedastic variant $\text{PG}(\sigma_\phi(y))$ consistently outperforms the fixed-variance version $\text{PG}(\sigma = 1)$ in both FID and accuracy, demonstrating the benefit of adaptive variance modeling. However, **P-Guide** is more sensitive to the choice of w and exhibits a narrower effective range; for example, on CIFAR-10 performance degrades at $w = 1.5$, while standard CFM remains stable and continues improving up to $w = 3.0$. Overall, **P-Guide** achieves competitive performance within a limited w range without incurring additional cost, whereas standard CFM attains better peak performance and robustness at the expense of doubled computation; we further show in Appendix C.4 that the guidance scale in P-Guide preserves the essential behavior of CFG.

Table 1: Quantitative results on CIFAR-10 and MNIST. All P-Guide results are obtained via a **single inference pass**. GFLOPs are reported per image generation (50 steps). FID and IS retain 3 significant figures; sFID retains 2 significant figures. Acc denotes classification accuracy (%).

Method	Pass	CIFAR-10					MNIST					
		w	FID ↓	sFID ↓	IS ↑	Acc (%) ↑	GFLOPs ↓	FID ↓	sFID ↓	IS ↑	Acc (%) ↑	GFLOPs ↓
CFM	1	1.0	9.44	0.0063	8.61	70.53	710.4337	5.87	0.0061	2.10	95.468	417.5978
CFM	2	1.5	4.00	0.0017	9.52	86.07	1420.8641	5.94	0.0061	2.10	99.608	835.1956
CFM	2	2.0	2.54	0.0004	10.10	92.34	1420.8641	6.12	0.0066	2.09	99.938	835.1956
CFM	2	3.0	3.72	0.0009	10.42	96.63	1420.8641	11.5	0.0120	2.06	99.982	835.1956
$\text{PG}(\sigma_\phi(y))$	1	0.9	9.22	0.0049	8.82	80.78	713.3849	2.39	0.0015	2.11	97.270	417.6066
$\text{PG}(\sigma_\phi(y))$	1	1.0	6.51	0.0026	9.07	83.99	711.9093	1.40	0.0007	2.11	98.974	417.6022
$\text{PG}(\sigma_\phi(y))$	1	1.1	10.48	0.0041	9.03	86.00	713.3849	2.18	0.0011	2.09	99.520	417.6066
$\text{PG}(\sigma_\phi(y))$	1	1.5	38.46	0.0164	7.65	76.75	713.3849	13.8	0.0098	2.02	99.962	417.6066
$\text{PG}(\sigma = 1)$	1	0.9	12.59	0.0081	8.32	68.53	713.3849	3.21	0.0029	2.13	97.480	417.6066
$\text{PG}(\sigma = 1)$	1	1.0	9.35	0.0057	8.61	72.49	711.9093	3.31	0.0030	2.13	98.216	417.6022
$\text{PG}(\sigma = 1)$	1	1.1	8.72	0.0044	8.67	76.69	713.3849	3.61	0.0032	2.12	98.606	417.6066
$\text{PG}(\sigma = 1)$	1	1.5	18.23	0.0060	8.69	81.12	713.3849	6.73	0.0055	2.08	99.510	417.6066

5.3 Scalability on ImageNet-1k

To assess scalability to high-resolution manifolds (256×256), we evaluate P-Guide using both a **U-Net** [34, 18] and a **Diffusion Transformer (DiT-B/2)**[29]. To reduce computational costs, the Stage-2 flow model is initialized with weights from a pre-trained CFM model [9] (originally trained for $\sim 10\text{M}$ steps) and further optimized for only 400K steps, requiring approximately 4% of the original training budget.

Architecture Comparison. Table 2 highlights that P-Guide introduces only a minimal computational overhead while maintaining a single-pass inference paradigm across both architectures. As evidenced by the **Size** column, this improvement is achieved by adding merely **1.247 MB** of conditional parameters, corresponding to a negligible storage increase ($< 0.5\%$ for U-Net). Crucially, this efficient adaptation is enabled by our heteroscedastic modeling (Stage 1), which provides **Adaptive Loss Attenuation** [19]. This mechanism stabilizes optimization during prior learning and facilitates fast convergence to a high-quality conditional representation, even under limited fine-tuning budgets.

Discussion on Sampling Quality Improvement. Similar to the original Classifier-Free Guidance theory[46], P-Guide demonstrates the ability to improve generation fidelity by adjusting the guidance scale w within a single inference pass. As shown in Table 2, increasing w from 1.0 to a moderate

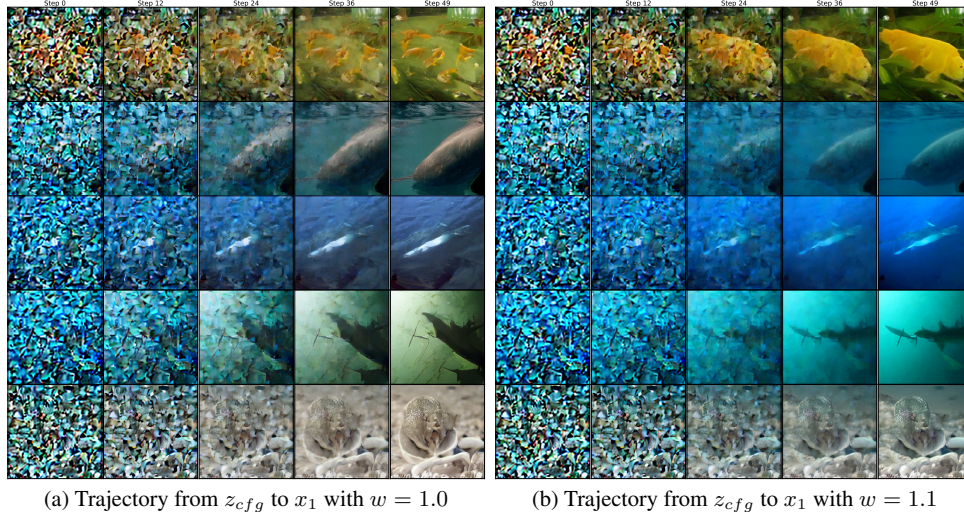


Figure 4: **Visual comparison of P-Guide trajectories on ImageNet.** Each row shows the evolution from prior ($t = 0$) to data ($t = 1$). Increasing the guidance scale ($w = 1.0 \rightarrow 1.1$) sharpens semantic structure from early steps, confirming effective trajectory-level control from the origin.

range (e.g., 1.1 for U-Net and 1.2 for DiT-B/2) leads to a clear reduction in FID, indicating that prior-space steering effectively sharpens the sample distribution. For example, the U-Net backbone FID improves from 27.78 to 22.33 at $w = 1.1$, while DiT-B/2 reaches its best performance of 25.07 at $w = 1.2$. We observe that the heteroscedastic and fixed-variance variants achieve comparable performance across different w , suggesting that both formulations provide similar guidance effects in this regime. However, further increasing w leads to degradation (e.g., $w = 1.5$), indicating a limited effective range of prior-space guidance. Overall, these results confirm that P-Guide can reproduce the quality improvement behavior of CFG within a single-pass framework, while maintaining constant computational cost.

Table 2: ImageNet-1k (256×256) performance across various guidance scales. All P-Guide results utilize a **single inference pass**. Model size is reported as backbone + PG module (AutoKL 79.779MB excluded). GFLOPs are reported per image generation (50 steps).

Scale w	U-Net + P-Guide				DiT-B/2 + P-Guide			
	FID ↓		GFLOPs ↓	Size (MB)	FID ↓		GFLOPs ↓	Size (MB)
	$\sigma = 1$	$\sigma_\phi(y)$			$\sigma = 1$	$\sigma_\phi(y)$		
1.0	28.40	27.78	3654.3964	388.55 + 1.247	32.84	33.68	2301.60	124.45 + 1.247
1.1	22.65	22.33	3655.8744	388.55 + 1.247	26.41	26.80	2303.08	124.45 + 1.247
1.2	22.67	23.01	3655.8744	388.55 + 1.247	24.61	25.07	2303.08	124.45 + 1.247
1.5	43.38	44.53	3655.8744	388.55 + 1.247	38.72	38.43	2303.08	124.45 + 1.247

6 Conclusion

We have presented P-Guide, a principled and parameter-efficient framework for single-pass conditional inference in Flow Matching. By shifting the guidance mechanism from iterative velocity-field extrapolation to the trajectory origin, P-Guide effectively mitigates the dual-pass computational bottleneck, achieving a $2\times$ throughput acceleration with negligible overhead. Our theoretical derivation establishes the trajectory-level approximation of prior-space steering, while heteroscedastic modeling provides robustness via adaptive loss attenuation. Crucially, P-Guide remains fully compatible with standard CFG (see Appendix C.4), acting as a complementary enhancement that preserves the effectiveness of traditional guidance signals without disrupting the underlying flow dynamics. We hope our work provides a scalable foundation for high-resolution generative systems and encourages further exploration of source-space control in continuous-time generative models.

References

- [1] Michael Samuel Albergo and Eric Vanden-Eijnden. Building normalizing flows with stochastic interpolants. In *International Conference on Learning Representations (ICLR)*, 2023.
- [2] Sanghyeon An, Minjun Lee, Sanglee Park, Heerin Yang, and Jungmin So. An ensemble of simple convolutional neural network models for mnist digit recognition, 2020. URL <https://arxiv.org/abs/2008.10400>.
- [3] Hmrishav Bandyopadhyay, Rahim Entezari, Jim Scott, Reshinth Adithyan, Yi-Zhe Song, and Varun Jampani. Sd3.5-flash: Distribution-guided distillation of generative flows, 2025. URL <https://arxiv.org/abs/2509.21318>.
- [4] Black-Forest-Labs. Flux.1, 2024. URL <https://blackforestlabs.ai/>.
- [5] Chen Chen, Pengsheng Guo, Liangchen Song, Jiasen Lu, Rui Qian, Tsu-Jui Fu, Xinze Wang, Wei Liu, Yinfei Yang, and Alex Schwing. CAR-flow: Condition-aware reparameterization aligns source and target for better flow matching. In *Neural Information Processing Systems (NeurIPS)*, 2026. URL <https://openreview.net/forum?id=idnW3BiZcV>.
- [6] Tian Qi Chen, Yulia Rubanova, Jesse Bettencourt, and David K Duvenaud. Neural ordinary differential equations. In *Neural Information Processing Systems (NeurIPS)*, 2018.
- [7] Yunfei Chu, Jin Xu, Wei Jiang, Lin Yang, Yang Wei, Jiaming Li, Shuailei Wang, Zejun Wang, Junyang Lin, and Jingren Zhou. Qwen-image technical report. *arXiv preprint arXiv:2405.12230*, 2024.
- [8] Hyungjin Chung, Jeongsol Kim, Geon Yeong Park, Hyelin Nam, and Jong Chul Ye. Cfg++: Manifold-constrained classifier free guidance for diffusion models. 2024. URL <https://arxiv.org/abs/2406.08070>.
- [9] Quan Dao, Hao Phung, Binh Nguyen, and Anh Tran. Flow matching in latent space. *arXiv*, 2023. URL <https://arxiv.org/abs/2307.08698>.
- [10] Jia Deng, Wei Dong, Richard Socher, Li-Jia Li, Kai Li, and Li Fei-Fei. Imagenet: A large-scale hierarchical image database. In *2009 IEEE Conference on Computer Vision and Pattern Recognition*, pages 248–255, 2009. doi: 10.1109/CVPR.2009.5206848.
- [11] Prafulla Dhariwal and Alexander Nichol. Diffusion models beat gans on image synthesis. *Neural Information Processing Systems (NeurIPS)*, 34, 2021.
- [12] Patrick Esser, Sumith Kulal, Andreas Blattmann, Rahim Entezari, Jonas Müller, Harry Saini, Yam Levi, Dominik Lorenz, Axel Sauer, Frederic Boesel, et al. Scaling rectified flow transformers for high-resolution image synthesis. In *International Conference on Machine Learning (ICML)*, 2024.
- [13] Weichen Fan, Amber Yijia Zheng, Raymond A. Yeh, and Ziwei Liu. Cfg-zero*: Improved classifier-free guidance for flow matching models. 2025.
- [14] Jiayang Gao, Tianyi Zheng, Jiayang Zou, Fengxiang Yang, Shice Liu, Luyao Fan, Zheyu Zhang, Hao Zhang, Jinwei Chen, Peng-Tao Jiang, Bo Li, and Jia Wang. C²fg: Control classifier-free guidance via score discrepancy analysis. 2026. URL <https://arxiv.org/abs/2603.08155>.
- [15] Kaiming He, Xiangyu Zhang, Shaoqing Ren, and Jian Sun. Deep residual learning for image recognition. In *IEEE Conference on Computer Vision and Pattern Recognition (CVPR)*, 2016.
- [16] Martin Heusel, Hubert Ramsauer, Thomas Unterthiner, Bernhard Nessler, and Sepp Hochreiter. Gans trained by a two time-scale update rule converge to a local nash equilibrium. In *Neural Information Processing Systems (NeurIPS)*, NIPS’17, page 6629–6640, Red Hook, NY, USA, 2017. Curran Associates Inc. ISBN 9781510860964.
- [17] Jonathan Ho and Tim Salimans. Classifier-free diffusion guidance. *arXiv preprint arXiv:2207.12598*, 2022.
- [18] Jonathan Ho, Ajay Jain, and Pieter Abbeel. Denoising diffusion probabilistic models. *Neural Information Processing Systems (NeurIPS)*, 2020.
- [19] Alex Kendall and Yarin Gal. What uncertainties do we need in bayesian deep learning for computer vision? In *Neural Information Processing Systems (NeurIPS)*, pages 5574–5584, 2017.
- [20] Alex Krizhevsky and Geoffrey Hinton. Learning multiple layers of features from tiny images. Technical Report 0, University of Toronto, Toronto, Ontario, 2009. URL <https://www.cs.toronto.edu/~kriz/learning-features-2009-TR.pdf>.

- [21] Y. Lecun, L. Bottou, Y. Bengio, and P. Haffner. Gradient-based learning applied to document recognition. *Proceedings of the IEEE*, 86(11):2278–2324, 1998. doi: 10.1109/5.726791.
- [22] Sang-gil Lee, Heeseung Kim, Changho Shin, Xu Tan, Chang Liu, Qi Meng, Tao Qin, Wei Chen, Yoonjoo Sung, and Tie-Yan Liu. Priorgrad: Improving conditional denoising diffusion models with data-dependent adaptive prior. In *International Conference on Learning Representations (ICLR)*, 2022.
- [23] Yaron Lipman, Ricky T. Q. Chen, Heli Ben-Hamu, Maximilian Nickel, and Matthew Le. Flow matching for generative modeling. In *International Conference on Learning Representations (ICLR)*, 2023.
- [24] Qihao Liu, Xi Yin, Alan Yuille, Andrew Brown, and Mannat Singh. Flowing from words to pixels: A noise-free framework for cross-modality evolution. In *IEEE Conference on Computer Vision and Pattern Recognition (CVPR)*, pages 2755–2765, 2025.
- [25] Xingchao Liu, Chengyue Gong, and qiang liu. Flow straight and fast: Learning to generate and transfer data with rectified flow. In *International Conference on Learning Representations (ICLR)*, 2023.
- [26] Simian Luo, Yiqin Tan, Longbo Huang, Jian Li, and Hang Zhao. Latent consistency models: Synthesizing high-resolution images with few-step inference, 2023.
- [27] Alexander Quinn Nichol and Prafulla Dhariwal. Improved denoising diffusion probabilistic models. In *International Conference on Machine Learning (ICML)*. PMLR, 2021.
- [28] Alexander Quinn Nichol, Prafulla Dhariwal, Aditya Ramesh, Pranav Shyam, Pamela Mishkin, Bob McGrew, Ilya Sutskever, and Mark Chen. Glide: Towards photorealistic image generation and editing with text-guided diffusion models. In *International Conference on Machine Learning (ICML)*, pages 16784–16804. PMLR, 2022.
- [29] William Peebles and Saining Xie. Scalable diffusion models with transformers. In *IEEE Conference on Computer Vision and Pattern Recognition (CVPR)*, 2023.
- [30] Dustin Podell, Zion English, Kyle Lacey, Andreas Blattmann, Tim Dockhorn, Jonas Müller, Joe Penna, and Robin Rombach. Sdxl: Improving latent diffusion models for high-resolution image synthesis. *arXiv preprint arXiv:2307.01952*, 2023.
- [31] Aditya Ramesh, Mikhail Pavlov, Gabriel Goh, Scott Gray, Chelsea Voss, Alec Radford, Mark Chen, and Ilya Sutskever. Zero-shot text-to-image generation. In *International Conference on Machine Learning (ICML)*, 2021.
- [32] Aditya Ramesh, Prafulla Dhariwal, Alex Nichol, Casey Chu, and Mark Chen. Hierarchical text-conditional image generation with clip latents. *arXiv preprint arXiv:2204.06125*, 2022.
- [33] Robin Rombach, Andreas Blattmann, Dominik Lorenz, Patrick Esser, and Björn Ommer. High-resolution image synthesis with latent diffusion models. In *IEEE Conference on Computer Vision and Pattern Recognition (CVPR)*, pages 10684–10695, 2022.
- [34] Olaf Ronneberger, Philipp Fischer, and Thomas Brox. U-net: Convolutional networks for biomedical image segmentation. In Nassir Navab, Joachim Hornegger, William M. Wells, and Alejandro F. Frangi, editors, *Medical Image Computing and Computer-Assisted Intervention – MICCAI 2015*, pages 234–241, Cham, 2015. Springer International Publishing. ISBN 978-3-319-24574-4.
- [35] Chitwan Saharia, William Chan, Saurabh Saxena, Lala Li, Jay Whang, Emily L Denton, Kamyar Ghasemipour, Raphael Gontijo Lopes, Burcu Karagol Ayan, Tim Salimans, et al. Photorealistic text-to-image diffusion models with deep language understanding. In *Neural Information Processing Systems (NeurIPS)*, volume 35, pages 36479–36494, 2022.
- [36] Shreshth Saini, Shashank Gupta, and Alan Bovik. Rectified CFG++ for flow based models. In *Neural Information Processing Systems (NeurIPS)*, 2026. URL <https://openreview.net/forum?id=NosdT1FHPv>.
- [37] Tim Salimans and Jonathan Ho. Progressive distillation for fast sampling of diffusion models. In *International Conference on Learning Representations (ICLR)*, 2022.
- [38] Tim Salimans, Ian Goodfellow, Wojciech Zaremba, Vicki Cheung, Alec Radford, and Xi Chen. Improved techniques for training gans. In *Neural Information Processing Systems (NeurIPS)*, NIPS’16, page 2234–2242, Red Hook, NY, USA, 2016. Curran Associates Inc. ISBN 9781510838819.
- [39] Jonas Scholz and Richard E. Turner. Warm starts accelerate conditional diffusion. 2025. URL <https://arxiv.org/abs/2507.09212>.

- [40] Jiaming Song, Chenlin Meng, and Stefano Ermon. Denoising diffusion implicit models. In *International Conference on Learning Representations (ICLR)*, 2021.
- [41] Yang Song and Stefano Ermon. Generative modeling by estimating gradients of the data distribution. *Neural Information Processing Systems (NeurIPS)*, 2019.
- [42] Yang Song, Jascha Sohl-Dickstein, Diederik P Kingma, Abhishek Kumar, Stefano Ermon, and Ben Poole. Score-based generative modeling through stochastic differential equations. In *International Conference on Learning Representations (ICLR)*, 2021.
- [43] Yang Song, Prafulla Dhariwal, Mark Chen, and Ilya Sutskever. Consistency models. In *International Conference on Machine Learning (ICML)*, 2023.
- [44] Christian Szegedy, Vincent Vanhoucke, Sergey Ioffe, Jon Shlens, and Zbigniew Wojna. Rethinking the inception architecture for computer vision. In *IEEE Conference on Computer Vision and Pattern Recognition (CVPR)*, pages 2818–2826, 2016. doi: 10.1109/CVPR.2016.308.
- [45] Wan Team. Wan: Open and advanced large-scale video generative models. *arXiv preprint arXiv:2502.17332*, 2025.
- [46] Hanyang Wang, Yiyang Liu, Jiawei Chi, Fangfu Liu, Ran Xue, and Yueqi Duan. Cfg-ctrl: Control-based classifier-free diffusion guidance. 2026. URL <https://arxiv.org/abs/2603.03281>.
- [47] Zhendong Yang, Zhe Li, Xiaojuan Jiang, Yuan Gong, Zehuan Yuan, Danpeng Zhao, and Chun Zhan. Masked generative distillation. In *European Conference on Computer Vision (ECCV)*, 2022.
- [48] Jingfeng Yao, Bin Yang, and Xinggang Wang. Reconstruction vs. generation: Taming optimization dilemma in latent diffusion models. In *IEEE Conference on Computer Vision and Pattern Recognition (CVPR)*, pages 15703–15712, 2025.

A Proof of trajectory-level approximation

In this section, we provide a detailed derivation showing that classifier-free guidance (CFG) applied in the prior space induces, to first order, the same trajectory perturbation as guidance performed directly in the velocity field. Throughout this appendix, we use the following notation:

- $z \in \mathbb{R}^d$ denotes the initial latent/prior state,
- $\Phi_t(z)$ denotes the flow map of the ODE at time t ,
- $v(x, t; z)$ denotes the velocity field induced by the initial state z ,
- $\epsilon \sim \mathcal{N}(0, I)$ denotes the shared base noise used to couple conditional and unconditional trajectories.

A.1 Preliminaries

Let $x \sim p(x)$ be the data distribution and let y denote the condition. The unconditional score is

$$s_t(x) = \nabla_x \log p_t(x), \quad (10)$$

and the conditional score is

$$s_t(x | y) = \nabla_x \log p_t(x | y). \quad (11)$$

By Bayes' rule,

$$s_t(x | y) - s_t(x) = \nabla_x \log p_t(y | x). \quad (12)$$

Hence, standard score-space CFG can be written as

$$s_{\text{cfg}}(x | y) = s_t(x) + w(s_t(x | y) - s_t(x)) = s_t(x) + w \nabla_x \log p_t(y | x). \quad (13)$$

A.2 Flow Matching as a Conditioned Dynamical System

In Flow Matching, generation is described by an ODE

$$\frac{dx_t}{dt} = v_\theta(x_t, t; z), \quad x_0 = z. \quad (14)$$

We denote the corresponding flow map by

$$x_t = \Phi_t(z). \quad (15)$$

Accordingly, the velocity along the trajectory is

$$v(x_t, t; z) = \frac{d}{dt} \Phi_t(z). \quad (16)$$

We consider two initial states constructed by the prior module:

$$z_c = \mu_\phi(y) + \sigma_\phi(y) \odot \epsilon, \quad z_u = \mu_\phi(\emptyset) + \sigma_\phi(\emptyset) \odot \epsilon, \quad (17)$$

where the same noise ϵ is used in both branches. This shared-noise coupling is essential: it allows us to compare conditional and unconditional trajectories as two perturbations around a common random base point.

A.3 Main Assumptions

We make the following mild assumptions.

Assumption 1 (Regular flow map). For each fixed t , the map $\Phi_t : \mathbb{R}^d \rightarrow \mathbb{R}^d$ is twice continuously differentiable in z .

Assumption 2 (Shared-noise coupling). Conditional and unconditional prior states are coupled by the same base noise ϵ , as in Eq. (17).

Assumption 3 (Local perturbation regime). We consider a first-order approximation regime with respect to the prior shift

$$\Delta z := z_c - z_u, \quad (18)$$

where higher-order terms in the Taylor expansion around z_u are neglected.

Assumption 4 (Optimal prior regression). The prior module is trained by Gaussian NLL, so that its mean prediction is the Bayes estimator under the model class:

$$\mu_\phi(y) \approx \mathbb{E}[x | y], \quad \mu_\phi(\emptyset) \approx \mathbb{E}[x]. \quad (19)$$

When the input is a noisy state x_t , the analogous conditional mean is $\mathbb{E}[x_0 | x_t, y]$.

A.4 A Useful Linearization Lemma

Lemma 1 (Local linear response of the flow map). *Under Assumption 1 and Assumption 3, for every fixed t ,*

$$\Phi_t(z_c) = \Phi_t(z_u) + J_t(z_u) \Delta z + R_t, \quad (20)$$

where

$$J_t(z_u) := \nabla_z \Phi_t(z) \Big|_{z=z_u} \quad (21)$$

is the flow Jacobian, and the remainder satisfies

$$\|R_t\| \leq C_t \|\Delta z\|^2 \quad (22)$$

for some constant C_t depending on the local curvature of Φ_t .

Proof. This is the standard second-order Taylor expansion of a C^2 map around z_u . Since Φ_t is twice continuously differentiable in z , we have

$$\Phi_t(z_c) = \Phi_t(z_u) + \nabla_z \Phi_t(z_u) (z_c - z_u) + O(\|z_c - z_u\|^2). \quad (23)$$

Letting $\Delta z = z_c - z_u$ gives the claim. \square

A.5 Velocity Perturbation Induced by Prior Shift

Lemma 2 (First-order velocity difference). *Under Assumption 1–3,*

$$v(x_t, t; z_c) - v(x_t, t; z_u) = \frac{d}{dt} (\Phi_t(z_c) - \Phi_t(z_u)) = \dot{J}_t(z_u) \Delta z + \tilde{R}_t, \quad (24)$$

where $\|\tilde{R}_t\| = O(\|\Delta z\|^2)$.

Proof. By definition,

$$v(x_t, t; z) = \frac{d}{dt} \Phi_t(z). \quad (25)$$

Taking the difference between the conditional and unconditional trajectories,

$$v(x_t, t; z_c) - v(x_t, t; z_u) = \frac{d}{dt} (\Phi_t(z_c) - \Phi_t(z_u)). \quad (26)$$

Using Lemma 1,

$$\Phi_t(z_c) - \Phi_t(z_u) = J_t(z_u) \Delta z + R_t. \quad (27)$$

Differentiating with respect to t yields

$$v(x_t, t; z_c) - v(x_t, t; z_u) = \dot{J}_t(z_u) \Delta z + \tilde{R}_t, \quad (28)$$

and $\tilde{R}_t = O(\|\Delta z\|^2)$ under the smoothness assumption. \square

A.6 Trajectory-Level First-Order Approximation

Theorem 1 (First-order trajectory approximation under shared-noise coupling). *Let z_c and z_u be defined by Eq. (17). Under Assumption 1–3, the conditional and unconditional trajectories satisfy*

$$x_t^{(c)} - x_t^{(u)} = J_t(z_u)(z_c - z_u) + O(\|z_c - z_u\|^2), \quad (29)$$

and their velocity difference satisfies

$$v_t^{(c)} - v_t^{(u)} = \dot{J}_t(z_u)(z_c - z_u) + O(\|z_c - z_u\|^2). \quad (30)$$

Consequently, both prior-space perturbations and velocity-space differences are driven by the same first-order direction $\Delta z = z_c - z_u$. In particular, for

$$z_{\text{cfg}} = z_u + w(z_c - z_u), \quad (31)$$

we obtain the induced trajectory perturbation

$$x_t^{\text{cfg}} = x_t^{(u)} + w J_t(z_u)(z_c - z_u) + O(\|z_c - z_u\|^2). \quad (32)$$

Moreover, the velocity-space CFG formulation

$$v_{\text{cfg}}(x_t, t) = v_t^{(u)}(x_t, t) + \tilde{w}(v_t^{(c)}(x_t, t) - v_t^{(u)}(x_t, t)) \quad (33)$$

induces a trajectory correction that, under a first-order linearization of the flow map, aligns with the same perturbation direction $J_t(z_u)\Delta z$, up to scaling differences between w and \tilde{w} arising from the nonlinear state-to-velocity mapping.

Proof. By Lemma 1,

$$x_t^{(c)} - x_t^{(u)} = \Phi_t(z_c) - \Phi_t(z_u) = J_t(z_u)(z_c - z_u) + O(\|z_c - z_u\|^2). \quad (34)$$

Similarly, by Lemma 2,

$$v_t^{(c)} - v_t^{(u)} = \dot{J}_t(z_u)(z_c - z_u) + O(\|z_c - z_u\|^2). \quad (35)$$

The key observation is that both state and velocity differences are governed by the same latent-space perturbation direction Δz , although they are expressed in different coordinate systems (state space vs. velocity field space).

For the guided prior

$$z_{\text{cfg}} = z_u + w\Delta z, \quad (36)$$

a first-order Taylor expansion yields

$$x_t^{\text{cfg}} = \Phi_t(z_u) + w J_t(z_u)\Delta z + O(\|\Delta z\|^2). \quad (37)$$

For velocity-space CFG, note that the correction

$$\delta v_t = \tilde{w}(v_t^{(c)} - v_t^{(u)}) \quad (38)$$

acts as an Eulerian perturbation of the vector field. The induced trajectory perturbation is governed by the variational dynamics

$$\frac{d}{dt}\delta x_t = \nabla_x v(x_t, t)\delta x_t + \delta v_t. \quad (39)$$

Under a first-order linearization of the flow map and the shared-noise coupling assumption, prior-space guidance and velocity-space CFG induce the same first-order perturbation direction in the linearized trajectory space spanned by $J_t(z_u)\Delta z$.

This implies that CFG can be equivalently implemented in the prior space, avoiding the need for dual forward passes required by velocity-space guidance. \square

A.7 Connection to the Conditional Score

To make the link to score-space CFG explicit, we connect the prior shift to the conditional score under a Gaussian perturbation interpretation.

Proposition 1 (Prior shift and conditional score). *Assume a Gaussian perturbation model at noise level σ_t , under which the posterior mean admits a score-based representation. Then the difference between conditional and unconditional estimators satisfies*

$$\mathbb{E}[x_0 | x_t, y] - \mathbb{E}[x_0 | x_t] = \sigma_t^2 \left(\nabla_{x_t} \log p_t(x_t | y) - \nabla_{x_t} \log p_t(x_t) \right) = \sigma_t^2 \nabla_{x_t} \log p(y | x_t). \quad (40)$$

Proof. Under a Gaussian perturbation model at noise level σ_t , the posterior mean can be expressed in score form as

$$\mathbb{E}[x_0 | x_t] = x_t + \sigma_t^2 \nabla_{x_t} \log p_t(x_t), \quad (41)$$

and similarly in the conditional case,

$$\mathbb{E}[x_0 | x_t, y] = x_t + \sigma_t^2 \nabla_{x_t} \log p_t(x_t | y). \quad (42)$$

Subtracting the two expressions yields

$$\mathbb{E}[x_0 | x_t, y] - \mathbb{E}[x_0 | x_t] = \sigma_t^2 \left(\nabla_{x_t} \log p_t(x_t | y) - \nabla_{x_t} \log p_t(x_t) \right). \quad (43)$$

Using Bayes' rule,

$$\nabla_{x_t} \log p_t(x_t | y) - \nabla_{x_t} \log p_t(x_t) = \nabla_{x_t} \log p(y | x_t), \quad (44)$$

which completes the derivation. \square

Combining Proposition 1 with Theorem 1, we interpret the prior-space shift induced by CFG as a first-order approximation to the conditional score direction. This provides a unified perspective linking prior-space guidance and score-based guidance under Gaussian perturbation, consistent with the trajectory-level equivalence established in Section A.6.

A.8 Adaptive Loss Attenuation in Training

We parameterize the prior module to output both mean and variance:

$$\mu_\phi(y), \quad \sigma_\phi^2(y) > 0. \quad (45)$$

Assuming a Gaussian likelihood, the training objective is

$$\mathcal{L} = \mathbb{E}_{x,y} \left[\frac{\|x - \mu_\phi(y)\|^2}{2\sigma_\phi^2(y)} + \frac{1}{2} \log \sigma_\phi^2(y) \right]. \quad (46)$$

Theorem 2 (Adaptive loss attenuation). *Under the NLL objective in Eq. (46), the gradient of the mean prediction is attenuated by the inverse variance:*

$$\nabla_{\mu_\phi} \mathcal{L} = -\frac{x - \mu_\phi(y)}{\sigma_\phi^2(y)}. \quad (47)$$

Therefore, large predictive uncertainty downweights the contribution of hard or noisy examples.

Proof. The terms depending on $\mu_\phi(y)$ are

$$\frac{1}{2\sigma_\phi^2(y)} \|x - \mu_\phi(y)\|^2. \quad (48)$$

Differentiating with respect to $\mu_\phi(y)$ gives

$$\nabla_{\mu_\phi} \mathcal{L} = \frac{1}{2\sigma_\phi^2(y)} \cdot 2(\mu_\phi(y) - x) = -\frac{x - \mu_\phi(y)}{\sigma_\phi^2(y)}. \quad (49)$$

Hence the gradient magnitude is inversely proportional to $\sigma_\phi^2(y)$, which realizes adaptive attenuation. \square

A.9 Stability of Velocity-Space Control

A practical reason for operating in velocity space is that the ODE is controlled directly at the level that determines the trajectory evolution. Consider a guided vector field

$$v_{\text{cfg}}(x, t) = v_u(x, t) + w(v_c(x, t) - v_u(x, t)). \quad (50)$$

If v_u and v_c are Lipschitz in x , then v_{cfg} is also Lipschitz, and the ODE remains well-posed. Moreover, by Grönwall's inequality, the trajectory deviation is bounded by

$$\|x_t^{\text{cfg}} - x_t^{(u)}\| \leq e^{Lt} \int_0^t \|w(v_c(x_s, s) - v_u(x_s, s))\| ds, \quad (51)$$

where L is a Lipschitz constant. This shows that velocity-space guidance provides a continuous and stable control signal over the entire integration path.

By contrast, directly mixing parameterizations such as means and variances changes the initial distribution in a way that need not preserve the shared-noise coupling structure. In particular, parameter interpolation does not in general correspond to a controlled perturbation of the vector field and therefore is not trajectory-equivalent to CFG in the ODE dynamics.

A.10 Final Unified Statement

We summarize the above results in the following compact formula. Under the denoising interpretation of the prior module and the local linear response of the flow map, the guided prior

$$z_{\text{cfg}} = \mu_\phi(\emptyset) + w(\mu_\phi(y) - \mu_\phi(\emptyset)) + \left[\sigma_\phi(\emptyset) + w(\sigma_\phi(y) - \sigma_\phi(\emptyset)) \right] \odot \epsilon \quad (52)$$

induces, to first order, the same trajectory perturbation as the corresponding velocity-space CFG. Therefore, a single guidance operation at initialization can replace repeated conditional/unconditional evaluations along the full trajectory, while preserving the leading-order guidance direction in the dynamical system. □

B Closed-Form CFG in Distribution Space and Failure Analysis

B.1 Closed-Form CFG in Distribution Space

Consider the unconditional and conditional initial distributions:

$$p_u(x) = \mathcal{N}(\mu_u, \sigma_u^2 \mathbf{I}), \quad p_c(x) = \mathcal{N}(\mu_c, \sigma_c^2 \mathbf{I}). \quad (53)$$

A natural distribution-level formulation of CFG is:

$$p_{\text{cfg}}(x) \propto p_u(x)^{1-w} p_c(x)^w, \quad (54)$$

which corresponds to a linear interpolation in log-density space:

$$\log p_{\text{cfg}}(x) = (1-w) \log p_u(x) + w \log p_c(x) + C. \quad (55)$$

Substituting the Gaussian log-density

$$\log p(x) = -\frac{1}{2\sigma^2} \|x - \mu\|^2 - \frac{1}{2} \log(2\pi\sigma^2), \quad (56)$$

and ignoring constants independent of x , we obtain:

$$\log p_{\text{cfg}}(x) = -\frac{1-w}{2\sigma_u^2} \|x - \mu_u\|^2 - \frac{w}{2\sigma_c^2} \|x - \mu_c\|^2 + C. \quad (57)$$

We now expand both quadratic terms explicitly:

$$\|x - \mu_u\|^2 = \|x\|^2 - 2\mu_u^\top x + \|\mu_u\|^2, \quad (58)$$

$$\|x - \mu_c\|^2 = \|x\|^2 - 2\mu_c^\top x + \|\mu_c\|^2. \quad (59)$$

Substituting back:

$$\begin{aligned} \log p_{\text{cfg}}(x) = & -\frac{1-w}{2\sigma_u^2}(\|x\|^2 - 2\mu_u^\top x + \|\mu_u\|^2) \\ & -\frac{w}{2\sigma_c^2}(\|x\|^2 - 2\mu_c^\top x + \|\mu_c\|^2) + C. \end{aligned} \quad (60)$$

Grouping terms by powers of x :

$$\begin{aligned} \log p_{\text{cfg}}(x) = & -\frac{1}{2} \left(\frac{1-w}{\sigma_u^2} + \frac{w}{\sigma_c^2} \right) \|x\|^2 \\ & + \left(\frac{1-w}{\sigma_u^2} \mu_u + \frac{w}{\sigma_c^2} \mu_c \right)^\top x + C'. \end{aligned} \quad (61)$$

Matching this with the canonical Gaussian form

$$-\frac{1}{2\sigma_{\text{cfg}}^2} \|x - \mu_{\text{cfg}}\|^2, \quad (62)$$

we obtain:

$$\frac{1}{\sigma_{\text{cfg}}^2} = \frac{1-w}{\sigma_u^2} + \frac{w}{\sigma_c^2}, \quad (63)$$

$$\mu_{\text{cfg}} = \sigma_{\text{cfg}}^2 \left(\frac{1-w}{\sigma_u^2} \mu_u + \frac{w}{\sigma_c^2} \mu_c \right). \quad (64)$$

Thus, CFG in distribution space results in a Gaussian whose mean and variance are jointly modified.

In the special case where $\sigma_u = \sigma_c = \sigma$, the above expressions simplify to:

$$\frac{1}{\sigma_{\text{cfg}}^2} = \frac{1}{\sigma^2}, \quad \mu_{\text{cfg}} = (1-w)\mu_u + w\mu_c. \quad (65)$$

This recovers the standard linear interpolation in mean space, consistent with the distribution-level CFG formulation in Eq. 63–64.

Moreover, this form matches the marginal distribution induced by P-Guide in Eq. 52, where the initial latent distribution is constructed as a convex combination of class-dependent components.

Therefore, the claim that distribution-level CFG is inherently inconsistent with ODE-based dynamics only holds in the general heteroscedastic case, and does not contradict the theoretical validity of the proposed P-Guide formulation under the homoscedastic setting.

B.2 Why Distribution-Level CFG Is Problematic

The key limitation of distribution-level interpolation is that it modifies the *shape of the density*, rather than directly influencing the *direction of trajectory evolution* induced by the underlying flow dynamics.

Sampling directly from $p_{\text{cfg}}(x)$ effectively:

- defines a new initial distribution,
- while keeping the dynamics $v(x_t, t | z)$ unchanged.

This leads to a mismatch between the sampling initialization and the velocity field. In particular, the shared-noise coupling assumption

$$(z_c, z_u) \text{ are no longer generated from the same base noise } \epsilon, \quad (66)$$

which is a key requirement in Section A, may no longer hold.

As a consequence, the trajectory-level interpretation of CFG becomes less accurate in the general heteroscedastic setting, as the guidance signal is partially decoupled from the underlying dynamics.

Table 3: Comparison between pretrained initialization and training from scratch for Stage-2 P-Guide. Both models are trained for 400K steps.

Initialization	FID ↓	GFLOPs ↓
From Scratch (400K)	49.03	2301.60
Pretrained + 400K	33.68	2301.60

B.3 Empirical Failure on MNIST

To empirically verify the mismatch identified in Section B, we conduct a controlled experiment on MNIST by directly sampling from the distribution-level CFG formulation $p_{cf_g}(x)$ instead of applying trajectory-level guidance.

Figure 5 presents a qualitative comparison between trajectory-level P-Guide and distribution-level CFG under the same initial noise and guidance scale ($w = 1.5$).

We observe that, although the distribution-level formulation modifies the marginal density, it fails to produce meaningful improvements in sample quality. In particular, the generated digits exhibit noticeable distortions and structural inconsistencies, while P-Guide preserves clear and semantically correct digit shapes.

This behavior remains consistent across different digit classes, indicating that increasing the guidance scale does not lead to systematic improvements under the distribution-level formulation.

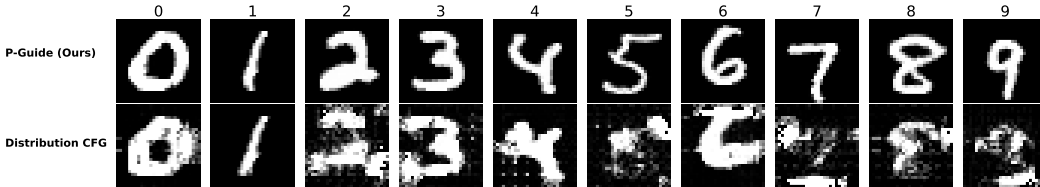


Figure 5: Comparison between trajectory-level guidance (P-Guide) and distribution-level CFG on MNIST under guidance scale $w = 1.5$. The distribution-level formulation leads to distorted and unstable samples, while P-Guide preserves semantic structure.

This failure is consistent with our theoretical analysis in Section A. Specifically, distribution-level CFG violates the shared-noise coupling assumption, which is essential for maintaining trajectory-level coherence between conditional and unconditional paths.

As a result, the geometric interpretation of CFG as a trajectory-level perturbation breaks down, and the method degenerates into a static density reshaping procedure that is not aligned with the underlying ODE dynamics.

These results further support the conclusion that effective guidance must operate at the trajectory level rather than directly modifying probability distributions.

C Additional Ablation Studies

C.1 Effect of Initialization: Pretrained vs. From-Scratch Training

We further investigate the impact of initialization on training efficiency for the Stage-2 flow model in P-Guide. Specifically, we compare two settings: (1) training the model from scratch, and (2) initializing from an existing pretrained flow model [9]. In both cases, the model is optimized for 400K steps under identical training configurations.

All experiments are conducted using the DiT-B/2 backbone with a single inference pass. Quantitative results are summarized in Table 3.

We observe that P-Guide can be successfully trained from scratch, achieving reasonable performance under a 400K-step training budget. However, initializing from a pretrained flow model consis-

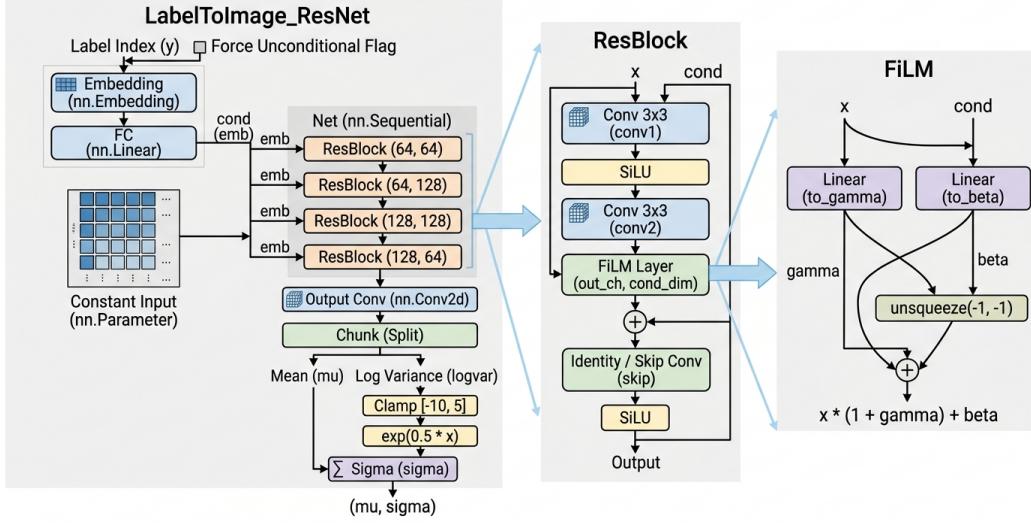


Figure 6: Architecture of the default P-Guide prior steering module (1.247 MB). The model consists of a lightweight conditional ResNet with FiLM modulation.

Table 4: Effect of prior module capacity on ImageNet-1k (256×256). All results use DiT-B/2 backbone with a single inference pass.

PG Module	Size (MB)	FID ↓	GFLOPs ↓
P-Guide (Default)	1.247	33.68	2301.60
P-Guide (Large)	12.5	34.34	2303.65

tently leads to better sample quality under the same number of optimization steps, indicating faster convergence.

This suggests that while P-Guide does not rely on pretrained models, it can effectively leverage existing flow models as a strong initialization in practice. Such initialization provides a convenient way to accelerate training of the Stage-2 model without altering the inference procedure.

Overall, these results demonstrate that P-Guide is compatible with both from-scratch and pretrained settings, while offering improved training efficiency when combined with existing flow models.

C.2 Influence of Prior Steering Module Capacity

To investigate whether increasing the capacity of the prior steering module $F_\phi(y)$ leads to further improvements, we compare the default lightweight design with an enlarged variant (PG-Large, 12.5 MB). The architecture of the default module (1.247 MB) is illustrated in Fig. 6, which adopts a compact conditional ResNet with FiLM modulation.

The larger variant scales up the model capacity by increasing both the number of residual blocks and the hidden channel width, while keeping the overall design identical.

Quantitative results are reported in Table 4. Despite a $10\times$ increase in parameter size, the performance remains comparable (FID changes from 33.68 to 34.34), while the computational cost remains nearly unchanged.

This observation indicates that the prior shift $z_c - z_u$ mainly acts as a low-dimensional directional signal in trajectory space, rather than requiring a high-capacity function approximator. In other words, the role of $F_\phi(y)$ is not to model complex distributions, but to provide a coarse yet effective steering direction.

Therefore, a lightweight conditional network is sufficient to capture the essential structure needed for single-pass guidance, leading to a favorable trade-off between performance and efficiency.

Table 5: Comparison of applying CFG to mean only vs. both mean and variance. Results are reported in FID (\downarrow) across different guidance scales w .

w	U-Net		DiT-B/2	
	Mean-only	Mean+Var	Mean-only	Mean+Var
1.1	22.33	22.09	26.80	26.71
1.2	23.01	23.14	25.07	24.75
1.5	44.53	47.62	38.43	38.31

Table 6: Joint evaluation of P-Guide and standard CFG on ImageNet-1k (256×256). Rows correspond to P-Guide scale w_{PG} , columns correspond to CFG scale w_{CFG} . All results use a U-Net backbone.

$w_{\text{PG}} \backslash w_{\text{CFG}}$	1.0	1.1	1.2	1.5	2.0
1.0	27.78	23.37	20.01	15.44	25.29
1.1	22.33	18.74	16.16	13.26	21.00
1.2	23.01	20.43	18.77	18.54	29.35

C.3 Effect of Applying Guidance to Variance

We investigate whether classifier-free guidance (CFG) needs to be applied to both the mean and variance of the conditional prior in P-Guide. The default formulation applies guidance to both components:

$$z_{\text{cfg}} = \mu_{\phi}(\emptyset) + w(\mu_{\phi}(y) - \mu_{\phi}(\emptyset)) + [\sigma_{\phi}(\emptyset) + w(\sigma_{\phi}(y) - \sigma_{\phi}(\emptyset))] \odot \epsilon. \quad (67)$$

We compare this with a simplified variant where CFG is applied only to the mean, while the variance remains conditional:

$$z_{\text{cfg}} = \mu_{\phi}(\emptyset) + w(\mu_{\phi}(y) - \mu_{\phi}(\emptyset)) + \sigma_{\phi}(y) \odot \epsilon. \quad (68)$$

All experiments are conducted using both U-Net and DiT-B/2 backbones with a single inference pass. Quantitative results are reported in Table 5.

We observe that applying CFG to the mean alone already achieves competitive performance, while incorporating variance guidance provides only marginal improvements in most cases. This suggests that the primary effect of guidance is captured by the mean shift in the prior space.

These findings further support our interpretation that P-Guide operates mainly through a directional control mechanism in the latent space, where the mean term dominates trajectory steering, and variance plays a secondary role.

C.4 Compatibility with Standard CFG

To further examine whether P-Guide is compatible with standard classifier-free guidance (CFG), we conduct an additional experiment where both mechanisms are applied jointly. Specifically, we first perform prior steering using P-Guide, and then apply standard CFG during ODE integration.

We evaluate combinations of guidance scales for P-Guide (w_{PG}) and standard CFG (w_{CFG}). Specifically, $w_{\text{PG}} \in \{1.0, 1.1, 1.2\}$ and $w_{\text{CFG}} \in \{1.0, 1.1, 1.2, 1.5, 2.0\}$, resulting in 15 configurations in total. Results on ImageNet-1k (256×256) with a U-Net backbone are reported in Table 6.

We observe that combining P-Guide with standard CFG does not lead to instability or degradation beyond the expected behavior of large guidance scales. In particular, moderate combinations (e.g., $w_{\text{PG}} \in [1.0, 1.2]$, $w_{\text{CFG}} \in [1.2, 2.0]$) remain stable and achieve competitive FID values.

These results suggest that P-Guide operates as a complementary mechanism to standard CFG, rather than interfering with its effect. This further supports our interpretation that prior-space steering and trajectory-level velocity extrapolation act on different stages of the generative process and can be composed without violating the underlying dynamics.

D Additional Qualitative Results

In this section, we provide additional qualitative results to complement the quantitative evaluations in the main text and Appendix C. These visualizations aim to further illustrate the behavior of P-Guide under different settings, including guidance strength, prior parameterization, and model architectures.

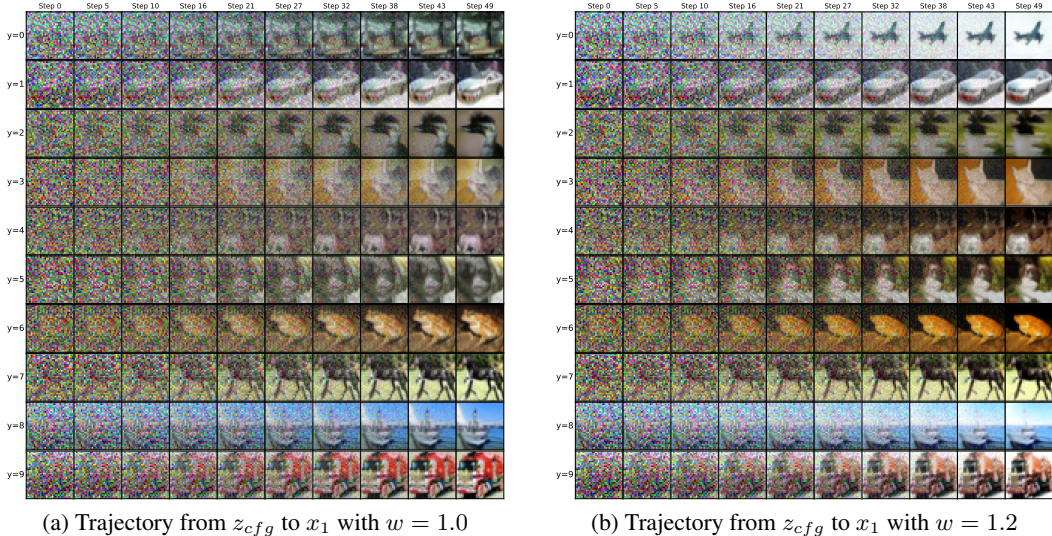


Figure 7: **Visual comparison of P-Guide generation trajectories on CIFAR-10.** Each row shows the evolution of a sample from its initial latent state ($t = 0$) to the final generated image ($t = 1$). Comparing $w = 1.0$ and $w = 1.2$, increasing the guidance scale leads to more semantically coherent structures emerging from the earliest stages of generation. This supports our hypothesis that modulating the initial latent state is sufficient to influence the entire sampling trajectory, without requiring iterative velocity-field extrapolation.

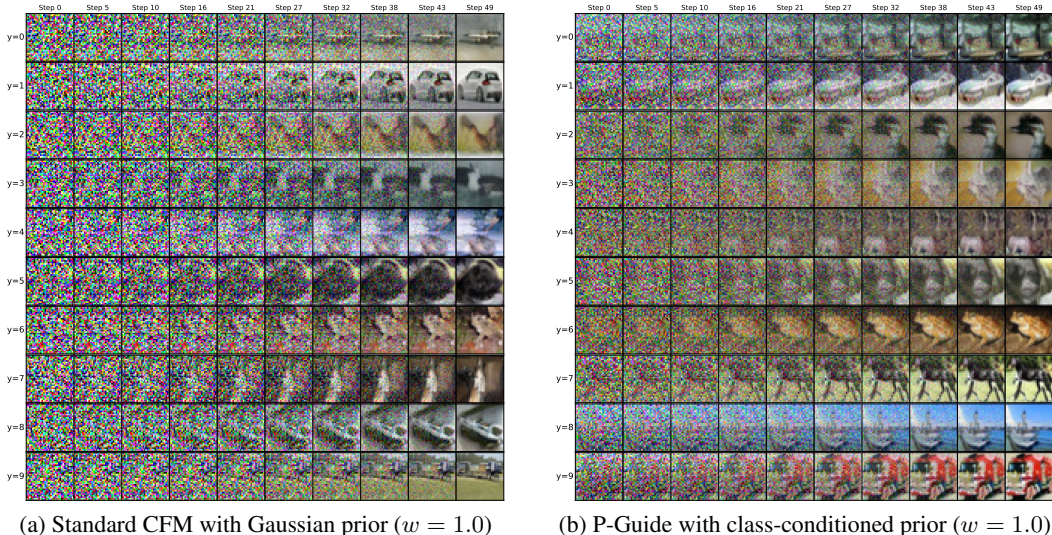


Figure 8: **Trajectory comparison under different initial latent distributions on CIFAR-10.** Each row visualizes the evolution of a sample from its initial state ($t = 0$) to the final generated image ($t = 1$). Standard CFM starts from a fixed Gaussian prior that is independent of class labels, resulting in less structured early-stage trajectories. In contrast, P-Guide initializes from a class-conditioned latent distribution, where different categories induce distinct starting points.

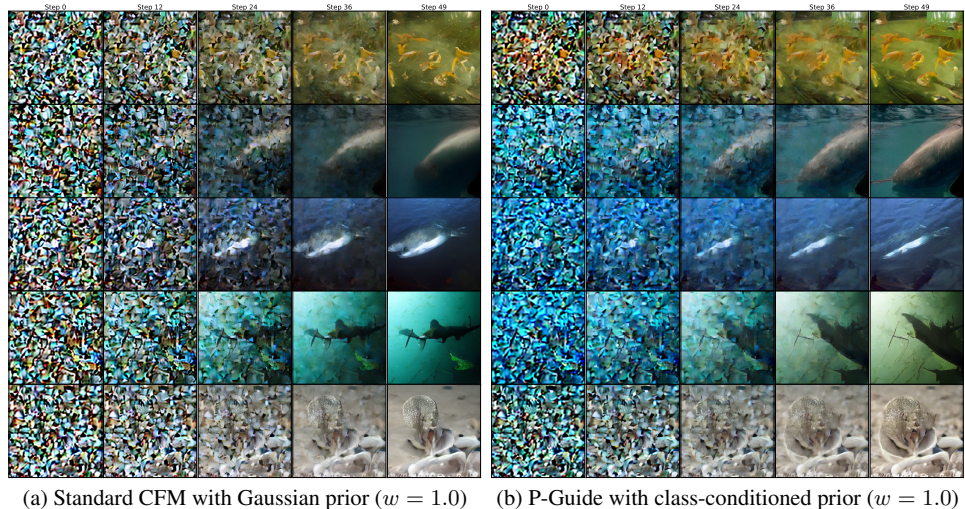


Figure 9: **Trajectory comparison under different initial latent distributions on ImageNet-1k.** Each row shows the evolution of a sample from its initial state ($t = 0$) to the final generated image ($t = 1$). As in CIFAR-10, standard CFM starts from a class-agnostic Gaussian prior, leading to less structured trajectories at early stages. In contrast, P-Guide initializes from a class-conditioned latent distribution, where different categories correspond to distinct starting points.

E Anonymous Code Release and Reproducibility

To facilitate reproducibility and enable further research, we provide an anonymous code release of P-Guide at:

<https://github.com/XinPeng76/P-Guide.git>

Code scope. The current anonymous release includes the core implementation of the proposed P-Guide method, in particular the prior-space steering module and the training pipeline used for ImageNet-1k experiments (see `train_imagenet256_DIT_PGGuide.py`). This implementation is sufficient to reproduce the training dynamics and validate the effectiveness of the proposed single-pass CFG inference paradigm.

F Statement on the Use of Large Language Models

During the preparation of this manuscript, large language models (LLMs) were used in a limited manner solely for language editing purposes, such as improving clarity, grammar, and academic style. All aspects of the research conception, methodological development, experimental design, analysis of results, and the scientific conclusions presented in this paper were carried out independently by the authors.